Corner-Sharing Tetrahedra for Modeling Micro-structure

Meera Sitharam, Jeremy Youngquist, Maxwell Nolan, Jörg Peters

University of Florida

Abstract

This paper introduces Corner-Sharing Tetrahedra (CoSTs), a minimalist, constraint-graph representation of micro-structure. CoSTs have built-in structural guarantees, such as connectivity and minimal rigidity. CoSTs form a space, fully accessible via local operations, that is rich enough to design regular or irregular micro-structure at multiple scales within curved objects. All operations are based on efficient local graph manipulation, which also enables efficient analysis and adjustment of static physical properties. Geometric and material detail, parametric or solid splines, can be added locally, on-demand, for example, for printing.

Keywords: corner-sharing tetrahedra, geometric constraint systems, constraint graphs, rigidity of frameworks, isostatic, metamaterial, micro-mechanics

1. Introduction and Motivation

Advances in composite materials and additive manufacturing permit, in principle, precise tailoring of micro-structure and shape at multiple scales to generate new synthetic materials with extraordinary properties. To design, analyze or optimize such artificial materials requires an efficient and versatile representation for manipulation of highly-detailed internal micro-structures. Pure B-rep or volumetric CSG representations are too bulky for non-uniform micro-structure spanning six orders of magnitude; when the basic constituents of the raw material are as fine and interact with the designed micro-structure ('lack of scale separation'); or to model micro-structure variance in manufacturing and irregularities due to wear.

Corner-Sharing Tetrahedra (CoSTs) are a low-cost, graph- and constraint-based representation for modeling and manipulating micro-structure, and to match macroscopic shape and physical properties. The *CoST graph* represents constraints (edges) between geometric primitives (vertices). The *CoST realization* must be embeddable in Euclidean space without overlaps. The advantage of such a minimal and abstract, essentially combinatorial representation independent of verbose geometry is not just efficiency, but versatility: a CoST can be interpreted to model trusses, tensegrities, packed incompressible disks or spheres, or a pinned-line incidence of cross-linking fibers that touch but are free to slide and rotate. CoSTs can therefore be used both for modeling natural or composite materials (whose minimally rigid, random micro-structure arises from internal material constraints); and - the focus in this paper - to design precise micro-structures. In all cases, a graph-based rigidity analysis enables efficient, initial engineering analysis before adding geometric detail and physical properties.

CoSTs are easily augmented to be *generically minimally rigid* (well-constrained), a graph property that is closely linked to the synonymous material property. Nature prefers supramolecular material to be minimally rigid, i.e. neither over-constrained (internally stressed) nor under-constrained (flex like a mechanism). A good way to generate a large family of CoSTs is to start with a regular, well-constrained lattice and apply local *flip* operations, i.e. locally change the underlying graph. Flips support both goals: *deterministic design* to match macroscopic shape and physical properties, and modeling grain boundaries, randomness and material defects of *natural composite structures*.

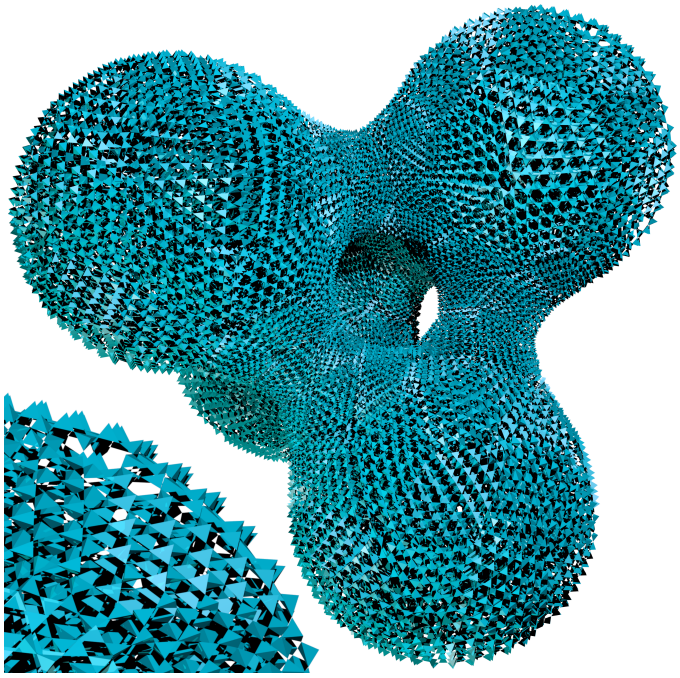

Figure 1: Micro-structure via Corner-Sharing Tetrahedra (CoSTs). The tetrahdra are rendered solid for easier visualization. See also [1].

Among regular, well-constrained lattices to initialize CoSTs, *Kagome* structures stand out. Due to their many desirable multi-physics properties, Kagome lattices have been extensively studied by material science experimentalists [2, 3, 4]. For example Kagome lattices have been shown to be maximally resilient, more so than variants of octet trusses, among statically determinate periodic (infinite) trusses [5]. Unlike most other truss-based lattices, infinite Kagome lattices are minimally rigid and can be hierarchically refined preserving structural properties and primitives, such as joints, from previous levels. Kagome structures have therefore been leveraged to derive theoretical predictions of physical behavior [6, 7, 8].

CoSTs generalize and extend Kagome structures to finite, non-periodic and irregular layout, while preserving their attractive properties including: the natural filling of tetrahedral domains (*short: tets*), easy joining of adjacent filled tets, and fitting to objects with curved boundaries and arbitrary topology, see Fig. 1. Associating spline geometry and material properties *on demand and only locally* with the CoST maximizes parallelism and minimizes storage overhead and makes slicing of a CoST-derived micro-structure for additive manufacturing highly efficient (Section 6).

The paper introduces and develops CoSTs with the following contributions.

- A class of constraint graph based, discrete representations, *Corner-sharing Tetrahedra (CoSTs)*, is defined to have baked-in generic independence and other desirable combinatorial properties.
- The *space of CoSTs* on n vertices, starting with Kagome structures, is shown to be rich. (In the bivariate case this space of CoSTs is proven to be as rich as all triangulations on n vertices.)
- A number of *operations with efficient algorithms* are defined to manipulate CoSTs and to preserve CoST properties (the space of CoSTs is closed under these operations):
    - Local graph operations, called *flips*, allow *accessing the full CoST design space* and modeling non-uniform micro-structures.
    - *Hierarchical CoST* refinement can be locally and selectively applied to access an extended space of CoSTs with more vertices.
    - CoSTs can be joined or glued to form larger CoSTs.
    - Mapping CoSTs by a free-form deformation allows *filling curved macro-shapes with micro-structure* to support practical design.
- CoSTs can be paired *on-demand and locally with spline-based* representations, both implicit and parametric.
- CoSTs can be systematically stiffened to guarantee minimal rigidity.
- Approximate, highly efficient computations of mass, stress and equivalent physical properties are based essentially on the graph. (Classical engineering analysis can be based on the associated geometry.)

The emphasis of this paper is on formally defining CoST spaces and establishing (proving) their richness, accessibility and closure under fundamental design operations. For illustrations, these operations have been implemented for bar-joint or equivalent body-pin constraint systems for deterministic design. (The operations readily extend to other types of constraint systems with the same constraint graph; and to modeling random micro-structure of composites.) In addition, the computation of stress based on the graph, of mass based on associated geometry, and slicing for 3D printing have been implemented. We envision future use within an iterative design-analysis optimization cycle.

1.1. Classification and comparison of micro-structure representations

Micro-structure representations can be sorted into three broad categories: continuous, continuous-from-discrete, and discrete.

Continuous functions and fields allow for many approaches to match boundary specifications, conforming, meshless, etc., see e.g. [9, 10]. Continuous representations are prevalent in the area of topology optimization: combining a nonlinear objective function with linearized constraints, topology optimization can link shape and micro-structure at multiple scales and is coupled with finite element physics computations to incorporate macroscopic shape and physical properties, see e.g. [11, 12, 13]. Continuous representations do *not easily encode or reveal connectivity*, such as provided by joining beams and struts, or their rigidity. Enforcing consistent material connectivity typically requires nonlinear or integer constraints.

To represent random micro-structure, *continuous-from-discrete* representations first generate pre-micro-structures via Poisson field smoothing and Voronoi subdivision based on a discrete set of positions of (ellipsoidal) shapes [14, 15]. These pre-micro-structures are subjected to simulation of sintering and other processes to yield 'effective micro-structures' [16, 15]. Tailoring the micro-structures of particulate matrix composites to macroscopic shape and physical properties then involves choosing controllable particle and matrix parameter values and a stochastic model of distribution over pre-micro-structures. Due to *limited control over the parameters and the need for a simulation* pipeline, this approach is generally used only for effective bulk properties of micro-structure [17], applicable only for large scale features of the filled macro-shape. Sample-based synthesis [18, 19] may provide an efficient shortcut.

CoSTs fall into the third class of *discrete* geometry representations that includes programmed lattices [20] and regular lattices, typically Cartesian grids of cubes, filled each with the same, possibly graded, triply periodic (minimal) surface type to create bulk properties [21, 22, 23]. The resulting 'thickened lattices' are analyzed via the finite elements approach. CoSTs (while permitting similar thickening) also differ in that they satisfy *built-in constraints*, permit non-periodic irregularities, and tailoring to bounded, curved objects. CoSTs belong a combinatorial rigidity class called 'frameworks' [24, 25]. Frameworks, called *D-reps* hereafter to avoid confusion, have been used by metamaterial physicists to model physical properties that can be reduced to flexes in essentially 2D (stacked) mechanisms [26, 27] and to investigate when jamming of particles occurs in randomly generated 2D composite materials [28, 29, 30]. Some of these D-reps can be viewed as special CoSTs that are regular and/or periodic. Flexibility of planar, periodic (infinite) D-reps was analyzed in [31, 32, 33, 34] and random bivariate D-reps that are CoSTs with periodic boundary conditions have been used to study percolation thresholds for rigidity in 2D glassy structures [35]. For (infinite) 3D zeolite structures, [36] use graph-based flexing conditions. However to date, the literature offers

- no design operations or tools for D-reps.
- no systematic characterizations or derivations of families or spaces of D-reps for micro-structure.
- no D-reps that one can compare to the CoSTs ability - via the design operations - to simultaneously

    (i) conform to curved outer geometric shape of arbitrary topology,
    (ii) guarantee built-in minimal rigidity (no self-stress),
    (iii) enable efficient analysis and adjustment of static physical properties,
    (iv) render smooth geometry locally, on demand, for e.g. for 3D printing, while avoiding intractably large storage.

CoSTs address all these issues.

1.2. Organization

Introducing a new representation has to cover many aspects. Section 2 formally defines CoSTs. Section 3 introduces operations for representing and designing micro-structure with CoSTs.

Section 4 explains and proves the properties of CoSTs. Section 5 focuses on how CoSTs enable the efficient computation of some key material properties. Section 6 demonstrates the efficiency of CoSTs when slicing CoST geometry for additive manufacturing.

2. CoSTs defined

A CoST is a special D-rep A typical D-rep consists of a *constraint graph* $G = (V, E)$ and a *realization* $\rho : v \in V \to \mathbb{R}^d$. For the purposes of this paper it suffices to think of the edges E as bars and the vertices V as joints, as in truss models. (Alternative interpretations as tensegrity or line-incidence constraint systems lead to models of packed incompressible spheres or cross-linking fibers.) While the vertices can be assigned on d-dimensional manifolds, for the purposes of this paper positions are assigned in $\mathbb{R}^d$. For micro-structures, the dimensions of interest are d=2 and d=3, i.e. *bi-variate and tri-variate* CoSTs.

There are several ways to define CoSTs. One could start with a concrete regular lattice in $\mathbb{R}^3$, apply the operations and algorithms of Section 3 and declare the outcome as the space of CoSTs. This section takes a more principled approach that, while more abstract, is ultimately more elegant and powerful to understand and manipulate CoSTs. We first define an idealized precursor of the CoST graph, the full-CoST graph.

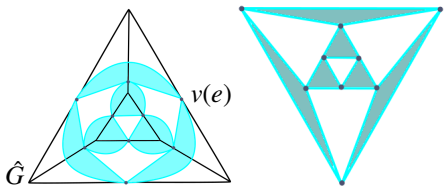

Figure 2: (*left*) A bivariate full-CoST graph (cyan; edges of graphs may be curved and cross) and its 3-regular graph (black; straight lines). The determining simplex graphs K_3 are the cyan triangles. (*right*) A bivariate CoST embedding (edges of embeddings are straight and the K_3, filled for visualization as in Fig. 1, must not overlap).

Fig. 2a illustrates (in cyan) a full-CoST graph in $d = 2$ dimensions. We start with a 3-regular (the black, straight-line) graph $\hat{G}$: every vertex of $\hat{G}$ has three neighbors. On every edge e, one point $v(e)$ is selected. The cyan, curved triangles, a.k.a. K_3 (simplex) graphs, are obtained by pairwise connecting the three $v(e)$ associated with a vertex. The union of the K_3 defines a full-CoST graph, with vertices $v(e)$. The construction establishes a bijection between the 3-regular graph and the full-CoST graph. Note that lines to display graphs can be curved and that none of the triangles of the original (black) 3-regular graph are part of the full-CoST graph.

Definition 1 (full-CoST graph, defining simplex graphs)**.** *A graph is k-regular if every vertex has k neighbors. K_n is the complete (simplex) graph of n vertices.*

Let $\hat{G}$ be a d+1-regular graph. Split each edge e of $\hat{G}$ by a vertex $v(e)$. For all edges e incident to a vertex u of $\hat{G}$, the $v(e)$ are pairwise connected by edges to form a defining simplex graph K_{d+1}. *The d-*variate full-CoST graph *is the union of all defining simplex graphs.*

For $d = 3$, a bijection relates tri-variate full-CoST graphs to 4-regular graphs, the defining K_4 sub-graphs are tetrahedra that are edge disjoint, and the tri-variate full-CoST graphs are 6-regular since each $v(e)$ is shared by exactly two K_4 spawned by the endpoints of e in $\hat{G}$.

In general, it is easy to check that a full-CoST graph has the following properties.

- (*CoST Bijection*) There is a bijection between d-variate full-CoST graphs and d+1-regular graphs.
- The copies of K_{d+1} that define the full-CoST graph are all edge disjoint.
- The d-variate full-CoST graphs are $2d$-regular since any $v(e)$ participates in two K_{d+1} corresponding to the endpoints of e in $\hat{G}$.

The full-CoST graph is almost, but not quite the graph of a CoST: real-world constraints interfere with simplicity. For example, if we prescribe generic edge lengths, as is needed for modeling trusses or sphere packings, then a full-CoST graph has no realization in $\mathbb{R}^d$. CoST graphs are therefore defined as pieces of full-CoST graphs, allowing for boundaries.

Definition 2 (CoST)**.** *The* graph *G of a CoST is a full-CoST graph, except that some vertices, called* boundary vertices*, are allowed to have between d and $2d$ edges. The* realization *of a CoST must satisfy the* CoST embedding *property: the defining simplices have a non-overlapping placement in $\mathbb{R}^d$.*

Fig. 2,*right*, illustrates the CoST embedding property.

To make the CoST minimally rigid, edges will be added by a boundary stiffening algorithm in Section 3. (The stiffened CoST graph is very close to a full-CoST graph but not quite a full-CoST graph.)

A CoST is *balanced* if it is a realization of a tensegrity D-rep with only struts or only ties, as, for example, for a material consisting of packed spheres. To resolve stresses at a vertex v, no hyperplane through v should have all edge vectors positioned on just one side. Therefore v is *balanced* if its direct neighbors cannot be confined to one half-plane. See Fig. 8.

A natural, balanced, well-studied bivariate CoST is the *bivariate Kagome* CoST. Starting with the equilateral triangulation T in $\mathbb{R}^2$ (Fig. 3, *left*) the *mid-point operation* ($\leftrightarrow$ in Fig. 3) yields (of a part of) the trihexagonal lattice (Fig. 3, *right*), a realization of the bivariate *Kagome* CoST.

A trivariate Kagome lattice can be defined by 4 cohorts of parallel planes, with three planes, one from each cohort, meeting at each point, and each K_4 defined by 4 planes one from each cohort. Fig. 4 shows a prototypical trivariate Kagome CoST with the K_4 rendered solid for ease of understanding. If we pick any fixed tetrahedron in $\mathbb{R}^3$, we can define four families of parallel bivariate Kagomes, each parallel to one face of the tetrahedron. Then the vertices of a *trivariate Kagome* realization are the intersection points of the four interleaving families.

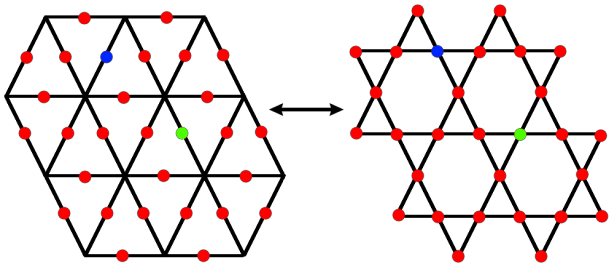

Figure 3: Mid-point Bijection: the mid-point operation yields a bijection between the triangulation and a CoST. Note the correspondence of the •.

More formally, we define the trivariate Kagome CoST constructively as follows (c.f. Fig. 4).

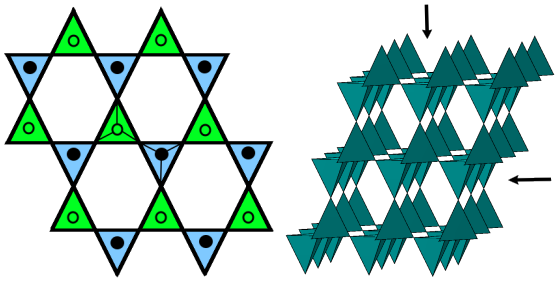

Figure 4: Construction of trivariate CoSTs by Definition 3. *left*: Points marked by ∘ are below, points marked by • are above the plane of the regular tri-hex bivariate CoST. *right*: There are four directions from which the trivariate Kagome looks like the bivariate Kagome.

Definition 3 (Stacked CoST, trivariate Kagome)**.** *A bivariate CoST is 2-colored if each triangle can be assigned one of two colors such that no two vertex-sharing triangles have the same color*

Consider a stack $C_1, C_2 \ldots$ of (green, blue) 2-colored bivariate CoSTs on parallel planes in $\mathbb{R}^3$ with successive layers related as follows. For i even, between every blue triangle in C_i and its corresponding blue triangle in C_{i+1}, introduce a new vertex (see • in Fig. 4a) and connect it to all six triangle vertices. This defines a pair of corner sharing tetrahedra. Do alike for i odd and green triangle pairs. The union of these defining tetrahedra is called a stacked trivariate CoST.

If the bivariate CoSTs are identical bivariate Kagome CoSTs but shifted relative to each other so that (see Fig. 4,right) each pair of corner sharing tetrahedra is defined by three common planes (through the common point) and two parallel planes (forming top and bottom triangles) then the stacked CoST is called trivariate Kagome*.*

A CoST is called *uniform* if all edge lengths are equal within a prescribed tolerance. This is natural for both designed metamaterials and naturally occurring materials (Silicon and Carbon based, sticky sphere colloids, jammed sphere composites). Kagome CoSTs are uniform.

As truss and wire woven structures, Kagome have been studied extensively and their physical properties have been characterized as superior to octet and other truss structures [37, 38, 5].

For conceptual clarity, it was necessary here and in the following to distinguish between *purely combinatorial* operations and operations requiring *realization*, e.g. purely involving graphs vs realizations satisfying the CoST embedding.

3. Operations for design with CoSTs

This section presents the default initialization of microstructure as a trivariate Kagome CoST filling a regular tetrahedron. Any tetrahedron (tet) output by a tetrahedral mesher, as in Fig. 5, can be filled by (an affine transformation of) a trivariate Kagome CoST restricted to the tet. But this raises several questions: how to consistently join the Kagome micro-structures between tets, how to reach a rich space of the CoST structures by local manipulation, how to ensure overall rigidity and how to associate 3D printable or bulk engineering-analyzable representations with the resulting CoST.

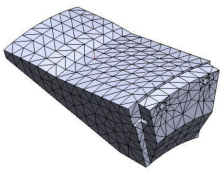

Figure 5: Standard partition into tets. Holes require many small tets.

The main focus of this section is therefore on establishing basic *operations on CoSTs*. Table 1 lists these basic operations: mapping the CoST to a given shape, modifying the CoST structure via flips, refining hierarchically, joining CoSTs, ensuring rigidity via stiffening, and associating surface and volumetric splines with a CoST. These operations are applied, possibly repeatedly, to create a design from an initial (Kagome or mid-point) CoST, and can be followed by analysis (Section 5, 6) to fashion a flexible design-and-analysis optimization cycle (that is beyond the scope of this paper). The exposition follows a natural order in which the operations might be applied in a work-flow. (One way to get a quick impression of the capabilities of CoST-based modeling is to browse the figures of the sub-sections.)

Initialization	**Operations**	**Analysis**
Section [3.1]	Section [3.2– 3.8]	Section [5, 6]
	Refine	
Kagome	Map (to curved)	Mass
Mid-point	Flip (re-connect)	Rigidity matrix
	Join	Graph Laplacian
	Stiffen	Slicing (3D print)
	Re-realization	
	Spline	

Table 1: Initialization, operations and computational tools that enable a design-analysis pipeline or cycle.

Flips, refinement, joining and mapping are carefully defined so that they can be applied in any order without loss of the CoST property (Theorem 13), i.e. so that the space of CoSTs is closed under these operations. Throughout, the important distinction is made between the *graph* operations and the (Euclidean) *realization* of the CoST.

3.1. Design space initialization

The default initialization fills an equilateral, unit tet with a trivariate Kagome CoST (see Fig. 7 *left*). The definition readily extends to a d-variate Kagome CoST.

Definition 4 (tet τ, Kagome)**.** *Denote the tet by τ. The vertices of the* Kagome *CoST of resolution ℓ are realized as points whose barycentric coordinates with respect to τ are*

$$(i_0, i_1, i_2, i_3)/(2\ell - 1) : \sum i_j = 2\ell - 1,\ i_j \in \mathbb{N}_0,\ i_j < 2\ell - 3$$
$$\text{exactly one of the } i_j \text{ is even.}$$

The resulting uniform, balanced, CoST is the default preimage of the micro-structure. For the purposes of this paper, this CoST is interpreted as a bar-joint D-rep, since they are versatile and can represent other types of D-reps with equivalent properties.

An alternative intialization, the mid-point CoST of any simplicial partition, uses the CoST bijection.

Definition 5 (Simplicial CoST graph, Mid-point CoST)**.** *A* simplicial *CoST graph G is derived from a partition of space into $d-$simplices as follows. Construct a dual graph $\hat{G}$ by associating a vertex with each simplex, and pairwise connect vertices whose simplices share a $d-1$ dimensional face. Then the graph G is the CoST bijection image of $\hat{G}$.*

A mid-point CoST *is an* embedded realization *of a simplicial CoST obtained by connecting the centroids of the* $d-1$*-dimensional faces of each* d*-simplex of a simplicial partition to form smaller* d*-simplices and removing the original simplicial partition.*

The bivariate Kagome is a mid-point simplicial CoST. The trivariate Kagome is not.

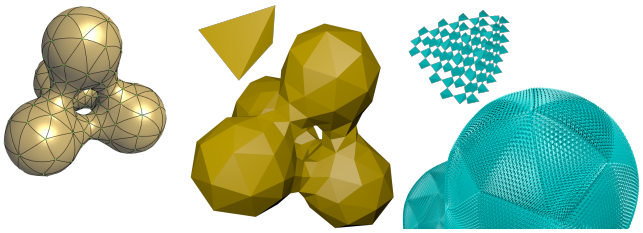

Figure 6: Surface of joined spheres (*left*) from [39], (*middle*) approximated by a partition into tets (one tet is replicated above) and (*right*) by a Kagome CoST, mapped by total-degree 3 polynomials that better capture the shape (one mapped Kagome tet is enlarged above).

3.2. Valid free-form deformations of CoSTs to match exterior shape

Given a polyhedral approximation of a surface there exist a number of meshing packages that can partition the enclosed solid into polyhedra, e.g. [40]. The most common option is to partition into tets T_i (see Fig. 6 *middle*). In the standard trade-off between polynomial degree and number of pieces, setting the error tolerance high allows the number of tets to be kept low while the original surface is better approximated by curving the exposed faces of the outer tets. For example, a sphere can be modeled by an octagon consisting of 8 tets with the 8 outer triangles mapped to the sphere Fig. 7. More recently, [39] directly optimized a curved tetrahedral partition to fit outer shape Fig. 6.

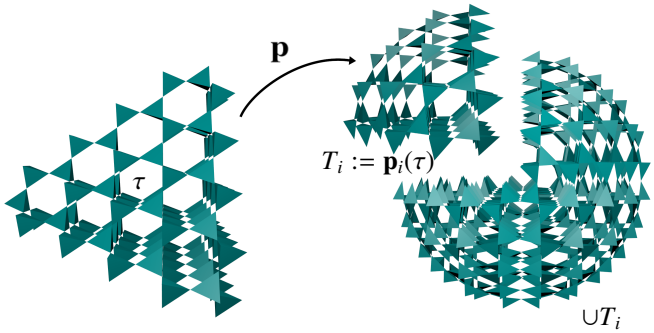

Figure 7: Mapping a Kagome CoST from its canonical domain τ (*left*) to a conforming shape $\mathbf{p}(\tau)$ (an octant of a sphere) and assembling the sphere by gluing mapped Kagome pieces.

The natural representation for a curved tetrahedron $\mathbf{p}(\tau)$ uses the total-degree Bernstein-Bezier form (see [41, 42]):

$$\mathbf{p}:\tau\in\mathbb{R}^3\to T\in\mathbb{R}^3,\quad \mathbf{p}(\mathbf{u}):=\sum_{|\alpha|=n}\mathbf{c}_\alpha\xi^\alpha,\quad \xi^\alpha:=\prod\xi_i^{\alpha_i},$$

$$\alpha:=(\alpha_0,\alpha_1,\alpha_2,\alpha_3)\in\mathbb{N}^4,\quad \xi:=(\xi_0,\xi_1,\xi_2,\xi_3),$$

$$\xi_i(v_j(\tau)):=\begin{cases}1 & \text{if } i=j,\\ 0 & \text{else}\end{cases},\ \xi_i(\tau)>0,\ \sum^n\xi_i=1.$$

Here α is a vector of non-negative indices adding to the polynomial degree n, ξ_j is the jth barycentric coordinate, i.e. varies linearly from 1 at the the vertex $v_j(\tau)$ and zero on all other $v_i(\tau)$. The product of powers of the ξ_i, form the individual multivariate Bernstein polynomials ξ^α scaled by the Bézier (de Casteljau) coefficients $\mathbf{c}_\alpha$.

A collection of points v in τ expressed in barycentric coordinates

$$\xi(v):=\begin{bmatrix}\tau\\ \mathbf{1}\end{bmatrix}^{-1}\begin{bmatrix}v\\ 1\end{bmatrix}\in\mathbb{R}^{d+1},\quad \mathbf{1}=[1,1,1,1]^t$$

is then deformed by $\mathbf{p}$. This *free-form deformation* provides a simple control cage for deforming highly detailed geometry. (Free-form deformation goes back at least to [43] and appears under the name of 'trivariate morphing' in the computer graphics literature.) In the following, we assume that the B-rep or CSG model has been partitioned into tets and that deformations $\mathbf{p}$ are *valid* in the sense that they preserve the CoST Embedding.

Importantly, the association of the CoST with curved geometry (and physical properties) is delayed until after the application of $\mathbf{p}$. Since free-form deformation is a composition of the trivariate map $\mathbf{p}$ with detail geometry $\mathbf{g}$, modeling $\mathbf{g}$ with standard tools of geometric design, i.e. as piecewise polynomial or rational spline, is costly: with $n_\mathbf{p}$ the polynomial degree of $\mathbf{p}$ and $n_\mathbf{g}$ the degree of the geometry, the polynomial degree of the deformed geometry is $n_\mathbf{p}n_\mathbf{g}$. For example, a tri-quadratic representation $\mathbf{g}$ has total degree 6 (the sum of degrees in the tensor-product directions) and the composition with a total degree cubic $\mathbf{p}$ is generically of total degree 18. For CoSTs the free-form deformation is applied only to the vertices and no edges are changed or deformed by $\mathbf{p}$. The mapping can be on-demand to minimize storage.

The art of free-form deformation lies in determining the map(s) $\mathbf{p}$ to least distort distances within T. Computing such (optimal) free-form deformations lies outside the scope of this introduction to CoSTs.

3.3. Designing CoSTs from Kagome seeds via flips

Starting with the Kagome CoST, more general, non-uniform CoSTs are generated by a local graph operation called a *flip*. A flip adds and removes edges while maintaining CoST graph properties. Flips are generally applied prior to mapping. However, since valid free-form deformations preserve the CoST property, flips can be applied post-deformation, e.g. to better conform to a given macro-shape or physical requirements (e.g. stress response), or to model stochastic material distribution of naturally occurring materials and particulate matrix composites.

For flips, too, it is important to distinguish between *graph* operations and the CoST *embedding* in Euclidean space.

Definition 6 (graph flip)**.** *For a* d*-variate CoST graph, a* flip at a vertex v *alters two defining simplices* A *and* B *that share* v*. Let* $a\in A$ *and* $b\in B$ *be distinct from* v*. A* flip *replaces all edges between* a *and other vertices in* A *by edges between* a *and vertices in* $B\setminus\{b\}$*; and all edges between* b *and other vertices in* B *by edges between* b *and vertices in* $A\setminus\{a\}$*.*

To preserve the CoST embedding and properties of the realization, one needs to apply sepcial kinds of flips, called CoST flip, modified flip and balanced flip.

Definition 7 (CoST flip, modified flip, balanced flip)**.** *A* CoST flip at a vertex v *is a graph flip at* v *that maintains all vertex positions and preserves the CoST embedding. (Only a balanced vertex* v *admits a CoST flip).*

A modified *CoST flip at a vertex* v *maintains all vertex positions other than* v *(see Fig. 8g). A* balanced *CoST flip allows perturbing vertex positions to restore the balanced property.*

The *graph flip* in a bivariate CoST graph G has a familiar interpretation (via a bijection proven in Theorem 11) as the well-known *diagonal flip* in a plane triangulation graph H (given two adjacent triangular facets $t_1 : v_1, v_2, v_3$ and $t_2 : v_2, v_0, v_3$, replace the shared diagonal edge (v_2, v_3) with the other diagonal (v_0, v_1)). To extend this interpretation to embeddings, the requirements of the following straightforward proposition have to be met by the diagonal flip in a plane triangulation and the corresponding CoST flip in its mid-point bivariate CoST.

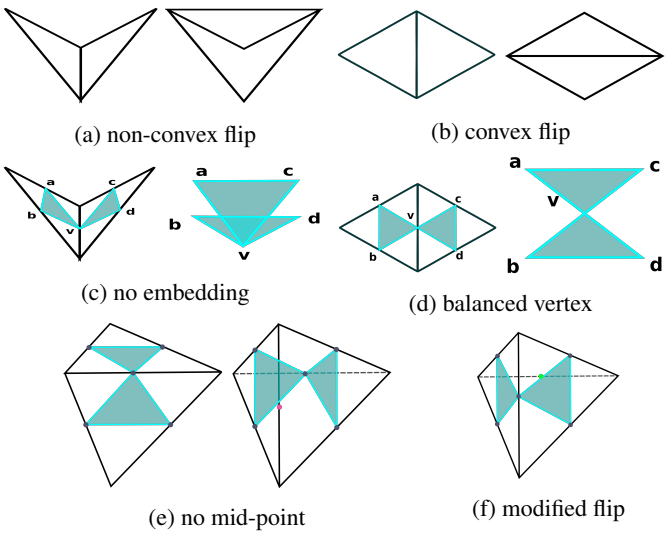

Figure 8: Balancing, Embedding, Mid-point operation. (a) A non-convex diagonal flip does not preserve the triangulation; (c) the corresponding graph flip at an unbalanced vertex destroys the CoST Embedding. (b) A convex diagonal flip corresponding to (d) a CoST flip at a balanced vertex. (b) and (d) illustrate, for a uniform triangulation, a commuting relation between the diagonal flip, the CoST flip and the mid-point operation; see Equation (1). (e) and (f) show that the relation fails for non-uniform triangulations. But (g) shows that the relation can be restored by a *modified* CoST flip that moves the CoST flip vertex to the midpoint of the new diagonal in the triangulation.

Proposition 8. *Consider a mid-point v of an edge e of a plane triangulation and let t_1, t_2 be triangles of the corresponding bivariate mid-point CoST that meet at v. Then the following are equivalent:*

- *v is balanced;*
- *the CoST flip at v yields a CoST;*
- *the quadrilateral formed by t_1 and t_2 is convex;*
- *the diagonal flip replacing e yields again a plane triangulation.*

Fig. 10a illustrates the effect of a diagonal flip on a triangulation and its corresponding mid-point CoST.

To preserve the stacking of a trivariate CoST such as Kagome any trivariate flip must be *induced by a bivariate flip* on a single set of parallel bivariate layers. This is illustrated in Fig. 9. The first flip of a trivariate Kagome at a vertex v is automatically an induced bivariate flip on one of the 3 bivariate layers incident at v. If the stacking is to be preserved on the once-flipped Kagome, any further trivariate flip must be induced by a bivariate flip on a single set of parallel bivariate layers. If the stacking need not be preserved, the once-flipped Kagome admits full trivariate flips in addition to those induced by bivariate flips on any of the four sets of parallel layers.

Perturbing Vertex Positions, Restoring balance, creating holes

Maintaining CoST vertex positions on a lattice during flips offers better control for free-form deformation of the CoST. But there are tradeoffs that motivated the definition of modified and balanced CoST flips in Definition 7. Maintaining vertex positions, a CoST flip at a vertex v maintains balance at v for future flips but can destroy balance at a neighbor vertex or the mid-point property of the a mid-point CoST. Moving each point towards the centroid of its neighbors restores balance. and moving v restores the mid-point property.

Also, after multiple flips, long edges will destroy uniformity, see Fig. 10b, a natural material constraint; repositioning can restore uniformity. Finally, vertex positions may have to be perturbed from special positions that prevent the built-in minimal rigidity of the CoST, see Theorem 14.

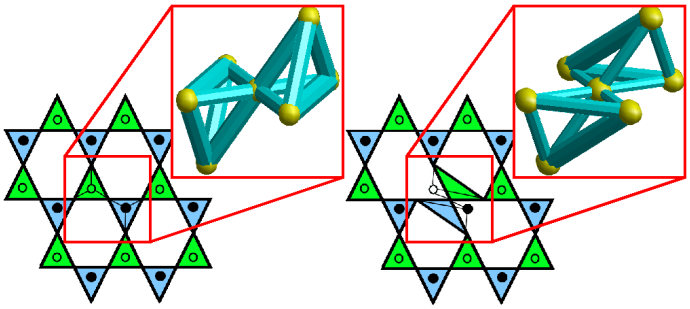

Figure 9: Induced bivariate flip in a stacked trivariate CoST. (*top-down view*: green tetrahedra face downward and connect to empty circles, blue tetrahedra connect upward to solid circles. (*enlargement*) Keeping the vertices in place, a flip locally reconnects the trivariate CoST.

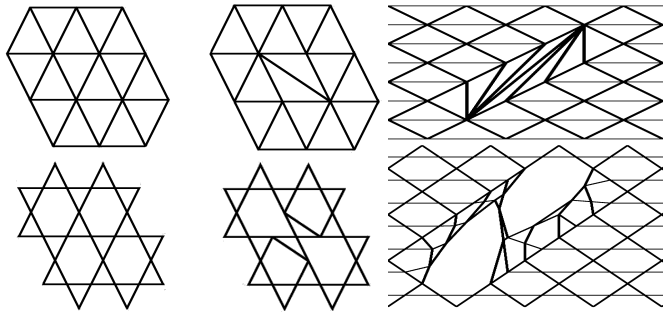

(a) triangulation (*top*) and its CoST (*bottom*)

(b) balanced nonuniformity

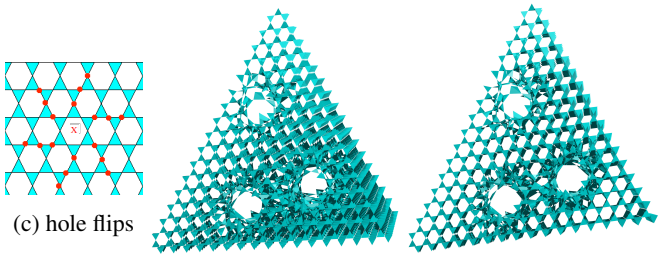

(c) hole flips

(d) hole through trivariate CoST (two views)

Figure 10: Effect of one convex diagonal flip on the equilateral triangulation and the corresponding CoST flip on a Kagome. (a) triangulation (*top*) and corresponding CoST (*bottom*). (b) a large nonuniformity in (*top*) the equilateral triangulation and (*bottom*) the corresponding CoST with restored balance. (c) Flips at vertices marked • in each 2d layer induce (d) cylindrical holes in a trivariate CoST.

Flips model Stone-Wales defects in many types of layered

crystals starting with equilateral triangular lattices – see Fig. 10b. The correspondence between triangulations on the points of the equilateral lattice and their mid-point CoSTs with points on the trihexagonal lattice can be leveraged for abstract models of defects and fractures. For example, a generalized Euclid's algorithm and Farey sequences can be used to generate a shortest sequence of neighboring convex diagonal flips that result a "defect" or "fracture" of any size (see Fig. 10b). (Combined with Section 5.1 this can provide a highly efficient way to obtain stiffness estimates while modeling fracture.) From a design perspective, nonuniformity can also be leveraged to introduce large cylindrical holes in the uniform trivariate Kagome, see Fig. 10d. Applying the planar flips at the vertices marked by • in Fig. 10c results in a circular hole with center × that, propagated along a line crossing the trivariate CoST yields Fig. 10d. Holes modeled at the CoST level frees an initial partition (cf. Fig. 5) from resolve those features and can so reduce the number of tets.

The flip also provides an efficient and principled way of modeling *random micro-structure with a predictable output distribution*. For example, we applied a Poisson process to set locations for the convex diagonal flip. A Markov process can then increase the probability of generating convex diagonal flips closer to previous flips in order to model fracture.

Flips can be applied before or after mapping to curved volumes via **p**.

3.4. Hierachical CoST Refinement

One way to refine a CoST is to increase ν in its Kagome initialization. The refinement discussed here is hierarchical refinement with a self-similar structure. This yields flexible control and scale-independence; and it supports efficient computation of static, linear physical properties via efficient block decompositions of the associated rigidity matrices (Section 5). Different levels and types of refinement can co-exist within a tet since the refinement operations retain all vertices of the previous level, preserve the vertex degree and create new edges based on new points on old edges. (This is akin to interpolatory stationary mid-edge subdivision and it similarly preserves the CoST structure while allowing fine-grained, local tailoring of mass and other physical properties.) The refinement operation is generally performed prior to free-form deformation. But, since it preserves the CoST embedding, it can also be performed after the flip and the free-form deformation e.g. for iterative adjustment.

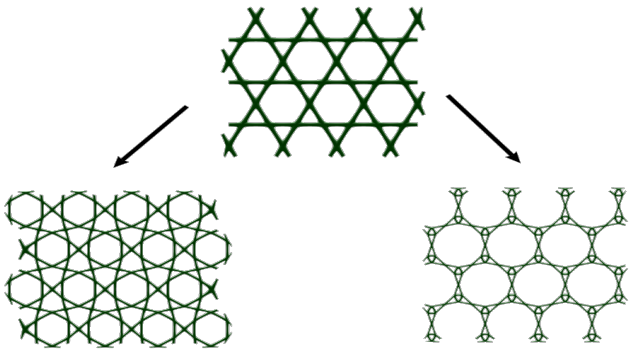

Figure 11: Rule R_1 (*left*) and R_0 (*right*)

Definition 9 (bivariate CoST refinement rules R_k)**.** *For each facet being refined, split each edge (u, v) into edges (u, z) and (z, v), adding a new vertex z. New edges connect the new vertices in clockwise ordering as a cycle. When applied to a corner-sharing triangle the rule is called R_0, for other facets R_1 (see Fig. 11).*

Both rules create two new triangles for each old vertex. When combined with initial flips to induce a random structure, n steps of the two refinement rules of Section 3.4 can model 2^n samples of random CoST micro-structure.

If F is a bivariate, equilateral and balanced CoST then

- applying Rule R_0 and positioning new vertices at the mid-point of the old bar ensures that the refined CoST is uniform in the refined region, (Rule R_1 destroys uniformity.)
- positioning the new vertex at the centroid of its neighbors ensures, for either rule, that the CoST is balanced.

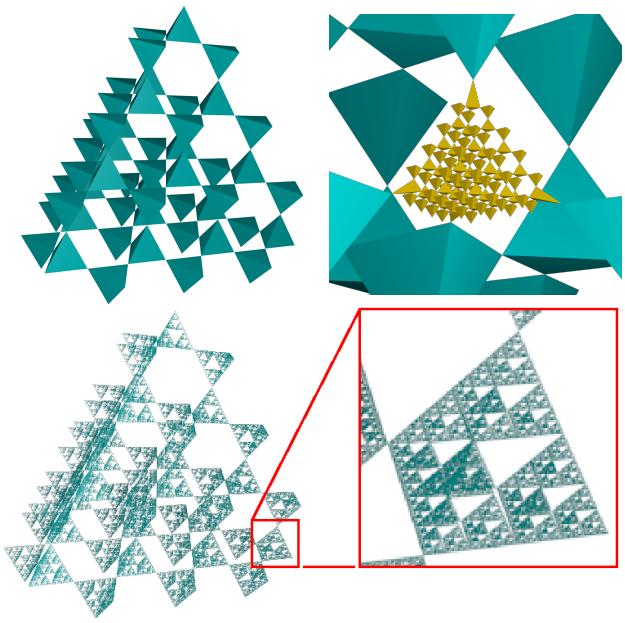

Figure 12: trivariate CoST refinement. *top*: local, adaptive, *bottom*: global, iterated.

Definition 10 (trivariate CoST refinement)**.** *The simplest refinement of trivariate CoSTs generalizes rule R_0 of the bivariate case by creating, for any K_4 (optionally all or a sub-set), four new K_4. (see Fig. 12).*

Alternatively, the stacked CoST can be assembled after the desired level of refinement has been performed on all bivariate CoST stacks.

The simplest refinement generalizes to d-variate CoSTs.

If an entire layer of K_4 is refined, two new layers arise between two parallel bivariate CoST layers. Alternatively, any chosen K_4 in the trivariate CoST can be replaced by a trivariate CoST. In all cases, balance is restored by moving each new point to the centroid of its neighbors. Within the refined region R_0 preserves uniformity.

3.5. Joining CoSTs

When joining the tets τ_i whose images T_i under $\mathbf{p}_i$ form the design object, the combined D-rep should again be a trivariate CoST, so that CoST operations can be performed after joining. If CoSTs in adjacent tets agree in refinement and position of boundary vertices (see Fig. 13 for bivariate CoSTs) boundary vertices have valence 3 and their pairwise merging yields the required valence 6 of the combined trivariate CoST graph (see Fig. 7,*right*). This is the case for the canonical initialization.

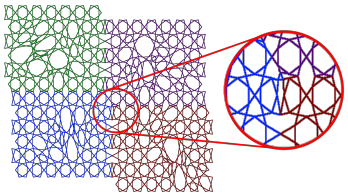

Figure 13: Joining bivariate CoSTs.

3.6. Re-realization

Joining CoSTs of differing density, changing connectivity, refinement and distortion by the maps f_i may require local bivariate re-computation of the node placement to make edge lengths more uniform. In general, solving bivariate distance constraints is a computationally demanding process equivalent to solving a quadratic polynomial system. This is an NP-complete challenge.

For CoSTs, however, sub-systems are small due to locality: updating geometric realizations requires only a recomputation in a small neighborhood of the merged vertices. Moreover CoSTs have a structure that makes them tractable by recent, nearly linear time algorithms, e.g. using CayMos [44, 45, 46]. This class of algorithms reduce the computation of realizations with known orientations, to searching the space of parameterized ruler-and-compass constructions and so improve efficient realization of the corresponding D-reps [47, 48, 49].

3.7. Stiffening: making CoSTs minimally rigid

The process of adding edges to boundary vertices to make the graph minimally rigid is called *stiffening*. Stiffening augments a d-variate CoST graph so that all but $\binom{d+1}{2}$ vertices have valence $2d$. Theorem 16 will prove that the stiffening scheme guarantees generic minimally rigidity. Minimal rigidity is desirable since it implies static physical properties of their material realizations (see Section 5).

Stiffening a *bivariate* CoST requires only increasing the boundary vertex degrees to 4. The stiffening algorithm simply connects the boundary vertices in sequence and leaving out 3 edges (see Fig. 14, *left*).

Stiffening a trivariate CoSTs is more challenging. Shared faces in an assembly of mapped CoSTs of the same refinement level join their boundary vertices to form vertices of valence 6. Each triangular face without partner, i.e. on the surface of the macro shape, can be stiffened by itself if and only if its boundary vertices can be connected by a 3-regular graph, i.e. if and only if ℓ in Definition 4 is chosen so that $\ell \bmod 4 \in \{1, 2\}$ (see Section 4.4).

Face stiffening proceeds by removing double 1d-layers of vertices from the outside of the face (linked by solid edges in Fig. 15) until one of six core patterns emerges (dashed), each of which has a 3-regular extension to form a 3-regular *stiffening graph* of extra stiffening edges. The stiffening graph is planar and has a uniform plane realization, ensuring a desired level of locality to prove minimal rigidity (in Section 4) and facilitate material realizations.

For the tet corners interior to the joined CoST, each of N (curved) tets T_i contributes one corner vertex whose valence 3 should be augmented to valence 6. (For a single tet, its four corners provide the degree deficit required for minimal rigidity.) One solution is to split each tet into four hexahedron and each hexahedron into six tets so that the resulting $6N$ corner vertices have a 3-regular cover. This is correct but clearly not efficient. A better, not immediately intuitive approach is to not connect the N corners to one another but to tie them down to their own tet. The

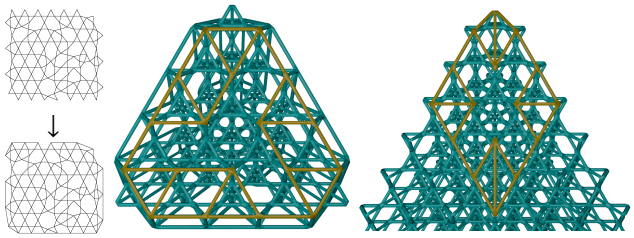

Figure 14: Boundary stiffening: (*left*) of a bivariate CoST; by adding yellow edges to stiffen (*middle*) a face of a trivariate CoST and (*right*) an internal corner.

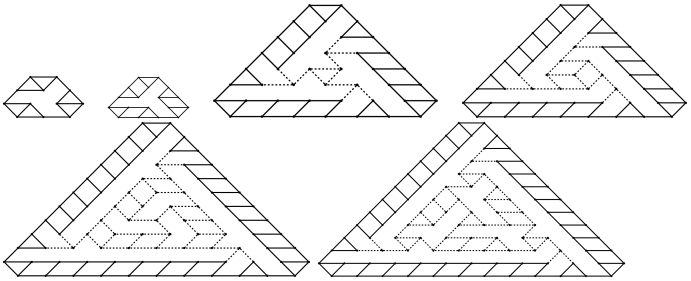

Figure 15: Face stiffening: the six possible core patterns (first two empty, other four dashed) framed to form a 3-cover.

internal corner stiffening algorithm forms cycles pairing up corners, and for each pair, splits apart 15 vertices that were joined in the common face and then adds the connections of a 3-regular graph on the 16 vertices, as illustrated in Fig. 14, *right*.

3.8. Associated surface and volume representations

Some operations in CAD systems, e.g. display or 3d printing, require a parametric boundary representation such as NURBS. Engineering analysis in 3-space is convenient when based on trivariate fields, e.g. a homogenized implicit representation of micro-structure.

The simplest *parametric* interpretation thickens the edges into beams. This representation often suffices for display. Fig. 16a shows a more sophisticated interpretation of the beams and nodes as a smooth spline surface of tensor-degree 2. This was used for additive layer deposition in 3d printing (see Fig. 23 in Section 6). Due to the regular connectivity of CoSTs, a simple, local algorithm fashions each half of a beam from four C^1-joined bi-quadratic patches on the fly. These bi-quadratic cylinder-like pieces then join to enclose the node and join C^1 with the pipe piece of the neighbor node, see Fig. 17. The construction is local, linear in the location of the nodes and offers parameters to locally thicken or thin the beams for continuous gradation. The arrow in Fig. 16a points to a modeled reinforcement of a particular pair of edges.

A smooth volumetric representation can be associated with a CoST by interpreting the nodes and their values (for example mass) as box-spline coefficients [50]. In two variables, the three directions of the trihex CoST are naturally associated with the convolution directions of the 3-direction box spline of the hat function [50]. Double convolution in each of the three directions yields the C^2 box spline whose generalization to irregular meshes is known as Loop subdivision [51]. Fig. 16b shows the filled zero level set of this bivariate field is of total degree 4 when setting the vertex values of the trivariate Kagome CoST to 1 and the empty grid locations to -1. The four planes of the trivariate Kagome suggest interpreting the vertices as control points of a 4-direction box spline (see e.g. [52]). Double convolution in the

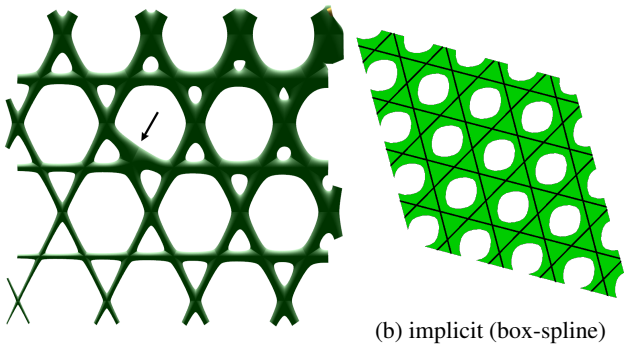

(a) parametric (spline) (b) implicit (box-spline)

Figure 16: (a) Gradation and local adjustment of the bi-quadratic parameterized surface representation associated with a geometric realizations of the constraint graph. (b) 3-direction box-spline level set.

directions yields a smooth volumetric field whose pieces are of total degree 5. Fig. 18a shows in yellow the zero level set when setting the node values to 1 and the empty grid locations to -1. Fig. 18b shows the Kagome CoST as blue tetrahedra superimposed on the level set, filling in the voids with value greater than zero. A small change to the shifts in the bivariate CoST layers in the construction of the trivariate Kagome results in the Tridymite structure of quartz-like material. Both Tridymite and Cristobalite (the standard Kagome) owe their strength to micro-structure.

4. Properties of the CoST design space

This section *formally proves* the key properties of the CoST design space:

- richness,
- accessibility by flips,
- closure under the operations of Section 3.2, 3.3, 3.4, 3.5, i.e. the operations can be applied in any order, and
- edge-augmentability to guarantee minimally rigidity (boundary stiffening).

Each property is characterized and proven in a separate subsection.

4.1. CoSTs form a rich space fully accessible via flips

The CoST bijection duality between d-variate full-CoST graphs and d+1-regular graphs has the following analogues.

Theorem 11 (Bijections). 1. *Embeddable d-variate CoST graphs are at least as rich as the dual graphs of d-dimensional simplicial partitions. (The dual graphs have valence at most d+1.)*

2. *There is a bijection between bivariate embeddable CoST graphs and plane triangulation graphs.*
   There is a bijection between bivariate embeddable CoST graphs and plane graphs of valence at most 3 with all interior vertices of valence 3.
3. *Let P be the set of equilateral lattice points in a regular triangular domain. Let P' be the corresponding set of mid-points forming a trihexagonal lattice. Let B and B' be the corresponding (well-defined) sets of boundary points. Let S be the set of triangulations with vertices in P and boundary vertices in B. Let S' be the set of CoSTs with vertices in P' and boundary vertices in B'. Then there is a bijection between S and S' called* Trihex Bijection.

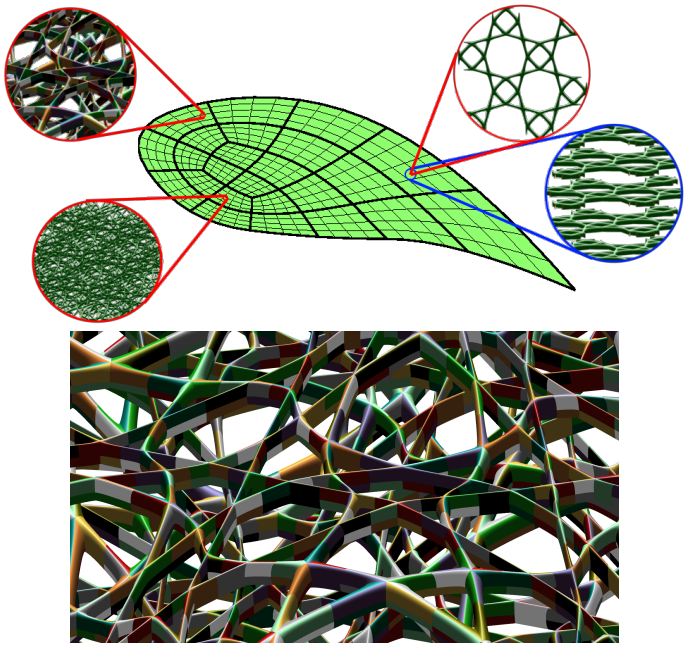

(a)

Figure 17: Stack-aligned slices through a CoST. (*top*) Enlargements: *red (right)* shows regular micro-structure, *red (left)* show nonuniform micro-structure viewed from top, *blue* shows the connected stack. (*bottom*) Close-up of the parametric splines associated with a bivariate CoST layer. Each spline patch is shown in a different color.

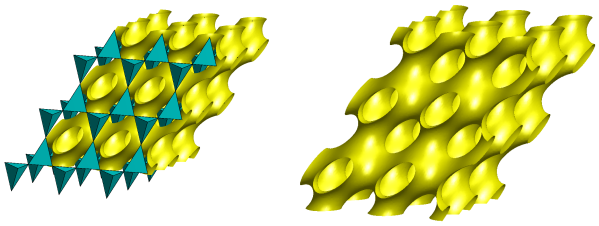

Figure 18: Zero level set (yellow) of the trivariate 4-direction box-spline initialized as values 1 at the nodes of the Kagome CoST (blue tetrahedra).

Fig. 19 illustrates a Trihex Bijection.

Proof. (1) The Mid-point Bijection (between d-dimensional simplicial partitions and their mid-point CoSTs) induces a bijection between dual graphs of simplicial partitions and simplicial CoST graphs; and shows the dual graphs to be embeddable with (non-intersecting) piecewise linear edges of at most two segments. The claim follows since simplicial CoST graphs are a subset of embeddable CoST graphs.

(2) By (1) the embeddable bivariate CoST graphs are at least as rich as the plane triangulation graphs. To prove the converse, take the centroids of the CoST triangles and connect them to their three vertices. This yields a 2-linear plane embedding of a graph H whose interior vertices have valence 3 and all vertices have valence at most 3. Fary's theorem [53] and a Tutte embedding of H extended to non-convex and multiple boundaries [54, 55] provide a straight-line embedding with convex interior faces. The dual of H is a plane triangulation graph whose edges can be made straight lines again by a Tutte embedding.

(3) Let S'' be the mid-point CoSTs of the triangulations in S. Therefore $S'' \subseteq S'$. Theorem 12 implies that S'' is exactly the class of CoSTs reachable from the bivariate Kagome using CoST

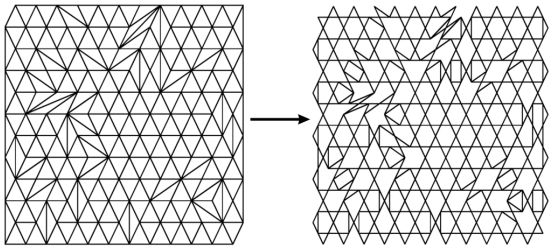

Figure 19: Trihex Bijection

flips. Theorem 12 also shows that all CoSTs in S' are reachable from the bivariate Kagome using CoST flips. Therefore $S' = S''$ and the obvious bijection between S and S'' is a bijection between S and S'. □

There are few embedding results in higher dimensions. Therefore it is not known if the converse of (1) is true, i.e, whether (2) generalizes to higher dimensions.

The following theorem uses the distinction, Definition 6 vs Definition 7, between graph flips, realizable CoST flips and modified CoST flips; and between general CoSTs and mid-point CoSTs.

Theorem 12 (Accessibility). 1. *The space of d-variate CoST graphs is connected by a sequence of graph flips. (The graphs may not be embeddable in $\mathbb{R}^d$ as CoSTs require).*
2. *The space of bivariate plane CoST graphs is connected via a sequence of graph flips (The graphs can be embedded in $\mathbb{R}^2$ as CoSTs, but the flips may not preserve point locations).*
3. *Let C be the space of bivariate CoSTs on a specified vertex set and specified boundary vertices of valence 2. C is connected by a sequence of CoST flips.*
4. *Let C be the space of bivariate mid-point CoSTs obtained from triangulations of the equilateral lattice with a specified boundary. The bivariate Kagome belongs to C and C is connected by a sequence of CoST flips.*
5. *Let C be the space of bivariate mid-point CoSTs obtained from triangulations of a specified point set with a specified boundary. C is connected by a sequence of modified CoST flips.*

Proof. (1) Any valence-preserving permutation of entries in an adjacency matrix can be achieved via block interchanges. A d-variate CoST graph flip is a block interchange. This provides the claimed path between the d-variate CoST graphs.

(2) Theorem 11 yields a bijection b between bivariate CoST graphs and plane triangulation graphs. Section 3 gives the correspondence between CoST graph flips and diagonal flips of triangulation graphs. A sequence f_i of diagonal flips allow reaching any plane triangulation graph from any other [56, 57, 58]. Then any bivariate CoST graph can be reached from any other by a sequence of flips $b^{-1} \circ f_i \circ b$.

(3) Replicate the proof of [59] that any plane triangulation on a point set with designated boundary can be reached from any other plane triangulation on the same point set and boundary via convex diagonal flips.

(4) A convex diagonal flip f on *any* triangulation T of the equilateral triangular lattice point set and the corresponding flip $\hat{f}$ on its mid-point bivariate CoST $m(T)$ preserve the mid-point correspondence:

$$\hat{f}(m(T)) = m(f(T)). \tag{1}$$

See Fig. 8. Thus for any triangulation T reachable from the uniform triangulation U by convex diagonal flips, $m(T)$ (on the trihexagonal lattice) is reachable from the bivariate Kagome using CoST flips. By [59], all triangulations with the same boundary B as U are reachable from U via convex diagonal flips.

(5) [Motivation for modified CoST flip.] Since the result by [59] applies to the set S of triangulations on *any* given point set with specified boundary, does the set S' of CoSTs reachable via CoST flips $\hat{f}$ from the mid-point CoST $m(T)$ of a triangulation $T \in S$ include all mid-point CoSTs of triangulations in S? I.e., is S' in bijection with S?

While the CoST $\hat{f}(m(T))$ preserves the same point set as $m(T)$, the mid-point CoST $m(f(T))$ after the corresponding convex diagonal flip f of T generally have a different point set. Conversely, no plane triangulation T with mid-point CoST $\hat{f}(m(T)$ may exist; or it is not guaranteed to be in S. I.e., the commutation in (1) between f, $\hat{f}$ and m fails. See Fig. 8e,f.

However, by modifying the position of the flip point v in the flipped CoST $\hat{f}(m(T))$ to the middle of the new diagonal in $f(T)$, we can access all mid-point CoSTs of triangulations in S. Specifically for the modified CoST flip $\tilde{f}$, the commutation $\tilde{f}(m(T)) = m(f(T))$ is restored. See Fig. 8g. This proves (5). □

The proof of (5) above adds another bijection to the list of Theorem 11: between S and the set of CoSTs reachable from the mid-point CoST $m(T)$ for $T \in S$ via modified CoST flips.

4.2. Closure of the CoST space under design operations

Closure under operations implies that the operations can be applied repeatedly and in any order. (This does not imply that they commute.) The operations in Section 3 were defined so that, with the help of Theorem 12(4),(5), the following statements are immediate.

Theorem 13 (CoST closure). 1. *d-variate CoSTs are closed under all types of CoST flips; and, for d = 2,3, under refinement and gluing.*
2. *Let L(F) denote the set of parallel bivariate layers defining a stacked trivariate CoST F. Stacked trivariate CoSTs are closed under induced bivariate CoST flips on any layer in L(F) and under simultaneous bivariate refinement of their L(F).*
   (a) *If any layer in L(F) is* restricted to a specified point set *closure only holds under bivariate CoST flips.*
   (b) *If any layer in L(F) restricted to be a* mid-point CoST *of a triangulation on a* specified point set*, the closure only holds under modified bivariate CoST flips. However, if the point set is the equilateral triangular lattice, closure also holds under bivariate CoST flips.*
3. *All above classes of CoSTs are closed under valid free-form deformations.*

4.3. CoSTs constraints are independent

There is a close relationship between combinatorial properties of D-reps and static physical properties of their material realizations. If the number of constraints matches the number of nodes (modulo the rigid motion group in $\mathbb{R}^3$) and if all (linearized) constraints are independent then a *generic* D-rep is (locally) *minimally rigid* (a.k.a. isostatic or well-constrained) [60]. Too few independent constraints indicate to *flexible* realizations. Note that a D-rep with dependent constraints can be simultaneously flexible and overconstrained. Dependent constraints result in self-stresses.

A D-rep class C is called *nice* if a characterization of generic rigidity using simple counting of edges and vertices is known.

Theorem 14 (Graph characterization of independence and minimal rigidity)**.** *Let $G = (V, E)$ be a constraint graph from a nice D-rep class C with constant l_C. G is generically* independent *in d dimensions if and only if for every sub-graph $G' = (V', E')$ of G*

$$|E'| \leq d|V'| - l_C.$$

G is minimally rigid in d dimensions if and only if G is independent *and*

$$|E| = d\,|V| - l_C. \tag{2}$$

Theorem 14 combines the known characterizations for classes C via the constant l_C. For example, when C is the bar-joint class in 2 dimensions, $l_C = 3$ since the trivial motion group in $\mathbb{R}^2$ consists of translation and rotation. Theorem 14 subsumes many rigidity results in two dimensions: bar-joint, tensegrity, body-pin (converted to bar-joint), direction line-incidence, point-line distance-angle D-reps [24, 61, 62, 28, 63] all have such a combinatorial characterization of generic independence and rigidity. A famous such proof for bar-joint D-reps is Hilda Geiringer's proof [64] of what is known as Laman's theorem [65]. For many nice D-reps, Theorem 14 generalizes beyond the Euclidean plane to geometric primitives and motions on a sufficiently smooth manifold.

While it is a well-known open problem to characterize generic rigidity of trivariate bar-joint D-reps, Theorem 14 with $d = 3$ does apply to special classes of bar-joint D-reps that are equivalent to to body-bar, body-hinge, body-pin and incidence systems. Luckily, trivariate CoSTs fall into such a special bar-joint D-rep class: a type of incidence system which is equivalent to a body-pin system [66, 67, 68]. Hence Theorem 14 with $d = 3$ applies.

Theorem 15 (CoST independence)**.** *d-variate CoSTs obtained from the d-variate Kagome using valid deformations, CoST flips and refinement rule R_0, are generically independent.*

Proof. The proof is based on Theorem 8.1.1 of [68] (independence of incidence systems), the transformation of trivariate bar-joint CoSTs into body-pin CoSTs (relying on the CoST embedding property: defining simplices do not intersect) and a further transformation to incidence systems. The transformation views a bar-joint simplex (being minimally rigid) as a body and must ensure that no two bodies share more than 1 pin and each body has at most $d + 1$ pins. These requirements are immediately met by the Kagome CoST since the simplices are its only bodies; and the CoST property ensures that no two simplices share more than one pin. The requirements also hold after flips and, by induction, after refinements. Now we can treat the structure as an incidence system and [68] shows independence of the CoSTs obtained from the Kagome via flips and refinement. Valid deformations do not alter generic properties. □

In fact, despite the non-genericity of its construction from four sets of parallel planes causing the pins on multiple bodies to lie on a plane, the trivariate Kagome CoST retains independence (i.e., there are no self-stresses).

4.4. CoSTs can be augmented to be minimally rigid

Theorem 16 (stiffening → rigid)**.** *The stiffening procedures described in Section 3 generate bivariate and trivariate generically minimally rigid structure.*

Proof. The stiffening described for bivariate CoSTs was shown in [69] to not generate any sub-graph violating the generic independence condition of Theorem 14. Since it has the correct number of edges, it meets the generic minimal rigidity condition. For the stiffening in the trivariate case, rigidity follows from the correct count as a bar-joint structure, provided independence can be shown. We start with the independence of the unstiffened CoST structure proved in Theorem 15. To deal with the newly added bodies (edges and triangles), we use not only the planarity but also uniformity and hence locality of the stiffening edges with respect to the CoST graph. Specifically, each new edge added during stiffening is between a pair of tetrahedra that are not corner-sharing (so that the property of two bodies sharing at most 1 pin is maintained), but locality is ensured as they share corners with a common tetrahedron. Each triangle added connects 3 tetrahedra where no pair shares the same corner-sharing neighbor. By induction, it follows that any proper substructure of the stiffened structure can still be treated as a body-pin system where any 2 bodies share at most one pin, and each body has at most 4 pins. We additionally use that all interior pins are shared by at most 2 bodies, and the maximum number of bodies sharing a boundary pin is 4, to extend the proof of Theorem 15. □

The above proof, that no body has more than 4 pins and no pair shares more than 1 pin in the trivariate CoST, relies on properties of the stiffening graph consisting of the added edges; in particular it is 3-regular and planar. This constrains ℓ in Definition 4 to $\ell \bmod 4 \in \{1, 2\}$ because a 3-regular graph on the $N := \binom{\ell+1}{2} - 3$ vertices of a Kagome face has $\frac{3N}{2}$ edges; so N must be even and hence $0 = \ell(\ell + 1) - 6 \mod 4 = (\ell + 3)(\ell - 2) \mod 4$.

As a consequence of Theorem 16, the only potential cause of dependent constraints and self-stresses is non-genericity. Since even highly non-generic Kagome are independent by Theorem 15 the effect of non-genericities depends on the boundary-stiffening scheme. The boundary stiffening schemes of Section 3 are not unique. Examples show that the minimal rigidity, dependencies and self-stresses of a non-generic stiffened CoST are sensitive to the actual boundary-stiffening scheme even though all satisfy the same generic rigidity conditions of Theorem 14.

5. Material properties

Material properties of D-reps ultimately depend on the associated continuous representation. However, many properties have a combinatorial characterization and can be determined from their constraint graph G leading to efficient algorithms.

For example, many nice classes in the sense of Theorem 14 have greedy algorithms for establishing if the graph is minimally rigid. Rigid components and rigidity percolation can determined by a special network flow algorithm called pebble game [48, 70, 71]. Furthermore, there are efficient algorithms for recursively decomposing such constraint graphs into maximal proper sub-graphs that are also minimally rigid. Even static physical properties that are not entirely combinatorial,, i.e. depend on D-rep geometry, admit highly efficient computations.

5.1. Static multi-physics: stiffness, Laplacian, resistance, mass via weighted graph Laplacian

Formally, the geometric constraint system is a set of polynomial equations $F = \{f_1, \ldots, f_m\}$ and variables $X = \{x_1, \ldots, x_n\}$. For an underlying constraint graph G, the *rigidity matrix* $R_G(p)$

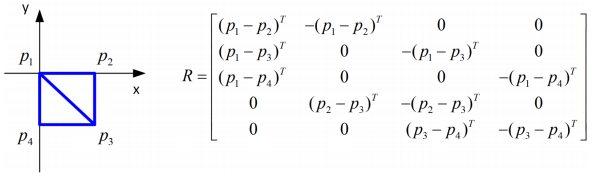

Figure 20: Example of a rigidity matrix (from [72]). Applying a force in the direction $(-1,-1)$ at p_2 compresses all outer edges and stretches the diagonal.

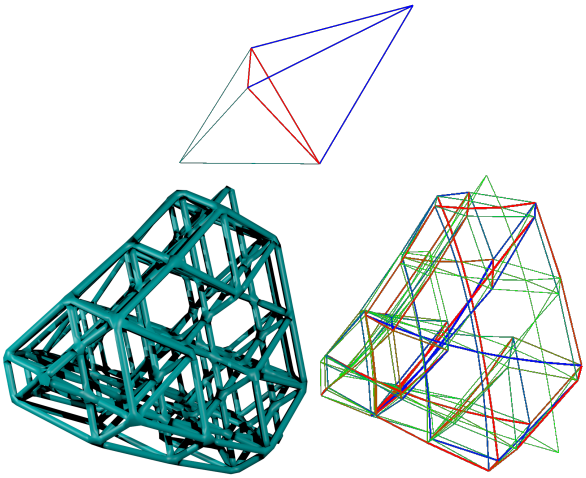

Figure 21: Stress distribution computed from the rigidity matrix of the CoST graph: compressive (blue – green – red) tensile; thickness according to absolute value of stress. *top*: force in the direction (-1,-1,-1) applied to the top right vertex. *bottom*: force in -z direction applied to the topmost vertex. (*left*) Stiffened CoST and (*right*) stress distribution.

is the Jacobian of F system with respect to X evaluated at instantiations $p(x_i)$ for variable x_i is

$$R_G(p) \in \mathbb{R}^{m\times n} : (i,j) \to \frac{\partial f_i}{\partial x_j}(p)$$

(see Fig. 20). When the constraints are quadratic, as for squared distance constraints, $R_G(p)$ is often referred to as the *linearization* of the constraint graph system. For generic p, row independence of $R_G(p)$ corresponds to local independence of the algebraic constraints of the original D-rep [60] And rigidity of the D-rep (G,p) is equivalent to $R_G(p)$ having maximum possible rank (over all D-reps (G,p)). Since maximum rank over p is attained at all generic p, rank and the associated properties of independence and rigidity of the original D-rep depend only on the constraint graph G.

Geometrically, any (infinitesimal) vector in the right nullspace of $R_G(p)$ represents an (infinitesimal) change to each primitive such that the resulting D-rep still satisfies all of the constraints. The left nullspace corresponds to an *equilibrium self-stress* of the system [73]. In the case of bar-joint or tensegrity D-reps, these stress vectors correspond to length-normalized forces on the bars, struts or ties – that cancel out at the joints, see Fig. 21. Moreover, the well-known stiffness matrix (when the bars/struts/ties are replaced by springs) has the same null space as the rigidity matrix. The stiffness matrix is therefore essentially a *weighted graph Laplacian* of the constraint graph G underlying the D-rep.

The Laplacian also yields the effective electrical resistance and analogously thermal resistance of appropriate physical realizations of the D-rep. Further related analogs include so-called topological insulator dielectric properties as well as photonic and acoustic properties related to G [2, 74, 75]. In short, rigidity, stiffness and Laplacian matrices of a D-rep, and their null spaces define stresses, flexes etc. and so provide an efficient way of computing effective multi-physical properties.

Crucially, refinement yields a recursive block structure in the rigidity, stiffness, Laplacian, and related matrices and so permits efficient computation at increasing levels of the hierarchy.

5.2. Mass Computations

Since every vertex of a CoST graph belongs to exactly two K_4 and every edge and face belong to exactly one, the perimeter, the area or volume of the tetrahedra provides an accurate measure of relative or proportional change in mass during refinement. Measuring change in mass under refinement is therefore a simple computation regardless whether the mass is at vertices, edges or faces of the bivariate or trivariate D-rep. For example, in $\mathbb{R}^2$, rule R_0 removes the central triangle from the coarser triangle reducing the mass by $\frac{1}{4}$; in $\mathbb{R}^3$ the reduction is $\frac{1}{2}$. Conversely, we can choose the refinement rule R_0 or R_1 at each step of the constructive refinement to achieve the desired change of mass.

When the associated surface is piecewise polynomial, it is straightforward, via the divergence theorem, to compute the exact volume contributed by each associated cylinder-like interpretation of edges. By symbolic computation, the contribution of each spline can be expressed as an inner product (less than 100 add or multiply per graph edge) of a precomputed vector representing the known structure and determinants of the node and its direct neighbors weighted by the parameters.

Mass enters the conversion of abstract D-rep properties into analogous physical material properties. For example, to achieve a physical stress s on a material realization of an abstract bar with stress t and length l in a bar-joint D-rep, the cross-sectional area A of the material bar must be lt/s. The desired strain, effective Young's modulus and density of the bar material follows from setting its mass.

6. Slicing for additive manufacturing

Slicing for additive manufacturing illustrates the efficiency of the CoST representation. For the anticipated extremely fine and non-uniform micro-structure, the memory requirement for computing entire slices for 3D printing is prohibitive. It is therefore natural to split the mapped CoST in $T := \mathbf{p}(\tau) \in \mathbb{R}^3$ by partitioning its regular pre-image (in τ) into sub-domains, e.g. filled or partially-filled cubes. The memory footprint is then restricted to the edges in one or more small sub-domains at a time. Specifically, intersecting just the six curved edges $\mathbf{p}((1-t)v_i(\tau)+tv_j(\tau))$, $t \in [0..1]$ of a curved tetrahedral image $\mathbf{p}(\tau)$ of a tet τ with the slicing plane returns an initial value t_0. Partitioning τ uniformly into sub-domains then allows slicing the image of the initial sub-domain – which is generated on demand and whose image easily fits into memory (see Fig. 22 and the video [76]). The exit boundaries determine a list of potential sub-domains to visit next and τ is completely sliced when the list is empty. The slicing test within a sub-domain queries whether the endpoints of an edge lie to either sides of the slicing plane – with a conservative margin that ensures that the associated curved geometry, e.g. beams in tensor-product Bézier form are sliced correctly (see the 3D prints of Fig. 23). The slicing is now reduced to a localized standard process that feeds to the printer only the relevant on-the-fly-generated curved geometry.

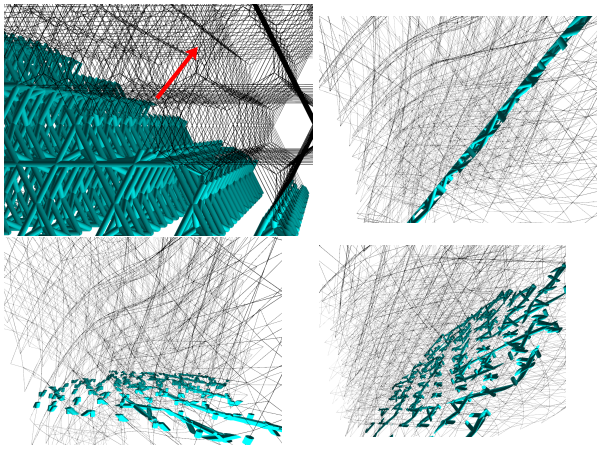

Figure 22: Slicing for additive layer deposition. (a) orthogonal to the red arrow in a Kagome CoST. (b,c,d) a slice through a mapped CoST (see also [76]).

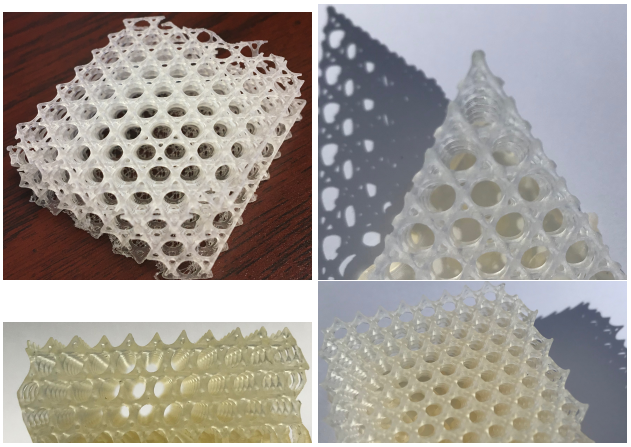

Figure 23: Printed CoSTs (not stiffened).

7. Conclusion

Corner sharing tetrahedra (CoSTs) are a new graph- and constraint-based representation, sufficiently light-weight to model micro-structure. Besides defining a foundation of operations (graph manipulation, hierarchical refinement, generation of non-uniformities according to distributions, augmentation, by stiffening, to guarantee minimal rigidity and combining with continuous representations) this paper emphasized formal definition of CoSTs and proofs of their properties, closure and accessibility. For example, CoSTs were shown to form a rich space: bivariate CoSTs are as rich as triangulations and fully accessible by graph manipulations so that initialization as (pieces of) Kagome lattices is a sound strategy.

The presented implementations were based on bar-joint or equivalent body-pin constraint systems applied in deterministic micro-structure design. While CoSTs can alternatively represent tensegrity, line-incidence, and similar constraint systems, these applications remain to be explored in more detail. The CoST's ability to model random non-uniformity through a controllable stochastic sequence of local flips implies potential for modeling and analyzing natural or composite materials whose random micro-structure arises from a variety of internal material constraints. Since a sequence of flips can model the emergence of material defects, CoSTs may be effective for simulating fracture.

We noted that a CoST's rigidity matrix and its left and right null spaces define stresses and flexes essentially from the graph. CoSTs therefore offer an initial, efficient analysis of static physical properties both aggregated or as precise distributions over a micro-structure-filled object. Since the self-similar hierarchical CoST refinement retains information from previous levels and results in a recursive block matrix, one can further improve computational efficiency and potential parallelism to form a flexible design-and-analysis optimization cycle.

Further research has to show how this discrete approach compares to finite element codes applied to localized B-rep or CSG representations of a CoST structure. For example, since 3D printed vertices lack the degrees of freedom of joints in a formal bar-joint structure, finite elements would establish whether stiffening - crucial for bar-joint structures - affects printed structures (beyond protecting from accidental damage due to exposed tetrahedra).

Future research has to establish whether CoSTs have efficiently computable Representative Volume Elements (RVEs) [77] that allow combining micro-structure analysis with standard analysis of bulk material and so form a bridge to classical topology optimization.

Acknowledgements This work was supported in part by DARPA HR00111720031, NIH R01 EB018625, NSF DMS-1563234 and NSF DMS-1564480.

References

[1] M. Sitharam, J. Youngquist, M. Nolan, J. Peters, Cost micro-structure, uRL: `https://www.youtube.com/watch?v=LwWOT8U2d-A`. Last visited 2019-04-25 (2019).

[2] H.-M. Guo, M. Franz, Topological insulator on the Kagome lattice, Phys. Rev. B 80 (2009) 113102.

[3] X. Yang, J. Bai, K.-J. Kang, T. Lu, T. Kim, Effective thermal conductivity of wire-woven bulk Kagome sandwich panels, Theoretical and Applied Mechanics Letters 4 (5) (2014) 051010, https://note.org/10.1063/2.1405110.

[4] J. Wang, A. Evans, K. Dharmasena, H. Wadley, On the performance of truss panels with Kagome cores, International Journal of Solids and Structures 40 (2003) 6981–6988.

[5] R. Hutchinson, N. Fleck, Microarchitectured cellular solids the hunt for statically determinate periodic trusses, ZAMM - Journal of Applied Mathematics and Mechanics / Zeitschrift fr Angewandte Mathematik und Mechanik 85 (9) (2005) 607–617.

[6] L. R. Meza, A. J. Zelhofer, N. Clarke, A. J. Mateos, D. M. Kochmann, J. R. Greer, Resilient 3d hierarchical architected metamaterials, Proceedings of the National Academy of Sciences 112 (37) (2015) 11502–11507, 10.1073/pnas.1509120112. `arXiv:http://www.pnas.org/content/112/37/11502.full.pdf`.

[7] A. Vigliotti, D. Pasini, Mechanical properties of hierarchical lattices, Mechanics of Materials 62 (2013) 32–43.

[8] Y. Sun, Q. Chen, N. Pugno, Elastic and transport properties of the tailorable multifunctional hierarchical honeycombs, Composite Structures 107 (2014) 698 – 710.

[9] F. Massarwi, J. Machchhar, P. Antolin, G. Elber, Hierarchical, random and bifurcation tiling with heterogeneity in micro-structures construction via functional composition, Computer-Aided Design 102 (2018) 148 – 159, special Issue on SPM 2018.
URL `http://www.sciencedirect.com/science/article/pii/S0010448518302264`

[10] S. Zeng, E. Cohen, Hybrid volume completion with higher-order bzier elements, Computer Aided Geometric Design 35-36 (2015) 180 – 191, geometric Modeling and Processing 2015.
URL `http://www.sciencedirect.com/science/article/pii/S016783961500031X`

[11] M. P. Bendse, N. Kikuchi, Generating optimal topologies in structural design using a homogenization method, Computer Methods in Applied Mechanics and Engineering 71 (2) (1988) 197 – 224, https://note.org/10.1016/0045-7825(88)90086-2.
URL `http://www.sciencedirect.com/science/article/pii/0045782588900862`

[12] P. Coelho, J. Guedes, H. Rodrigues, Multiscale topology optimization of bi-material laminated composite structures, Composite Structures 132 (2015) 495 – 505, https://note.org/10.1016/j.compstruct.2015.05.059.
URL http://www.sciencedirect.com/science/article/pii/S0263822315004420

[13] P. G. Coelho, H. C. Rodrigues, Hierarchical topology optimization addressing material design constraints and application to sandwich-type structures, Struct. Multidiscip. Optim. 52 (1) (2015) 91–104, 10.1007/s00158-014-1220-x.
URL http://dx.note.org/10.1007/s00158-014-1220-x

[14] S. Kale, F. A. Sabet, I. Jasiuk, M. Ostoja-Starzewski, Tunneling-percolation behavior of polydisperse prolate and oblate ellipsoids, Journal of Applied Physics 118 (15) (2015) 154306, 10.1063/1.4933100. arXiv:https://note.org/10.1063/1.4933100.
URL https://note.org/10.1063/1.4933100

[15] M. A. Groeber, M. A. Jackson, Dream.3d: A digital representation environment for the analysis of microstructure in 3d, Integrating Materials and Manufacturing Innovation 3 (1) (2014) 5, 10.1186/2193-9772-3-5.
URL https://note.org/10.1186/2193-9772-3-5

[16] G. Varghese, M. Moral, M. Castro-Garca, J. J. Lpez-Lpez, J. R. Marn-Rueda, V. Yage-Alcaraz, L. Hernndez-Afonso, J. C. Ruiz-Morales, J. Canales-Vzquez, Fabrication and characterisation of ceramics via low-cost dlp 3d printing, Boletn de la Sociedad Espaola de Cermica y Vidrio 57 (1) (2018) 9 – 18, https://note.org/10.1016/j.bsecv.2017.09.004.
URL http://www.sciencedirect.com/science/article/pii/S0366317517300948

[17] T. Kanit, S. Forest, I. Galliet, V. Mounoury, D. Jeulin, Determination of the size of the representative volume element for random composites: statistical and numerical approach, International Journal of Solids and Structures 40 (13) (2003) 3647 – 3679, https://note.org/10.1016/S0020-7683(03)00143-4.
URL http://www.sciencedirect.com/science/article/pii/S0020768303001434

[18] X. Liu, V. Shapiro, Sample-based synthesis of two-scale structures with anisotropy, Computer-Aided Design 90 (2017) 199–209.

[19] X. Liu, V. Shapiro, Multiscale shapematerial modeling by composition, Computer-Aided Design 102 (2018) 194 – 203, special Issue on SPM 2018. doi:https://doi.org/10.1016/j.cad.2018.04.024.
URL http://www.sciencedirect.com/science/article/pii/S0010448518302446

[20] A. Gupta, K. Kurzeja, J. Rossignac, G. Allen, P. S. Kumar, S. Musuvathy, Designing and processing parametric models of steady lattices, Tech. rep., GVU Technical Report;GIT-GVU-2018-02 (06 2018).

[21] J. Panetta, Q. Zhou, L. Malomo, N. Pietroni, P. Cignoni, D. Zorin, Elastic textures for additive fabrication, ACM Trans. Graph 34 (4) (2015) 135:1–135:12.
URL http://doi.acm.org/10.1145/2766937

[22] I. Maskery, L. Sturm, A. Aremu, A. Panesar, C. Williams, C. Tuck, R. Wildman, I. Ashcroft, R. Hague, Insights into the mechanical properties of several triply periodic minimal surface lattice structures made by polymer additive manufacturing, Polymer 152 (2018) 62 – 71, sI: Advanced Polymers for 3DPrinting/Additive Manufacturing. doi:https://doi.org/10.1016/j.polymer.2017.11.049.
URL http://www.sciencedirect.com/science/article/pii/S0032386117311175

[23] Autodesk, Withinlab (accessed April 10 2019).
URL http://www.withinlab.com/case-studies/new_index10.php

[24] J. E. Graver, B. Servatius, H. Servatius, Combinatorial rigidity, Graduate studies in mathematics, American mathematical society, Providence (R.I.), 1993.

[25] M. Sitharam, J. Sidman, A. StJohn (Eds.), Handbook of Geometric Constraint Systems Principles, Discrete Mathematics and Its Applications, 604 pages, CRC Press LLC, 2018.

[26] J. Paulose, A. S. Meeussen, V. Vitelli, Selective buckling via states of self-stress in topological metamaterials, Proceedings of the National Academy of Sciences 112 (25) (2015) 7639–7644, 10.1073/pnas.1502939112. arXiv:http://www.pnas.org/content/112/25/7639.full.pdf.

[27] J. Paulose, B. Chen, V. Vitelli, Topological modes bound to dislocations in mechanical metamaterials, Nature Physics 11.

[28] A. Donev, Jammed packings of hard particles, Ph.D. thesis, Princeton University (2006).

[29] A. Donev, S. Torquato, F. H. Stillinger, R. Connelly, Jamming in hard sphere and disk packings, Journal of Applied Physics 95 (3) (2004) 989–999.

[30] A. B. Hopkins, F. H. Stillinger, S. Torquato, Disordered strictly jammed binary sphere packings attain an anomalously large range of densities, Phys. Rev. E 88 (2013) 022205, 10.1103/PhysRevE.88.022205.

[31] V. Kapko, M. M. J. Treacy, M. F. Thorpe, S. D. Guest, On the collapse of locally isostatic networks, Proceedings of the Royal Society of London A: Mathematical, Physical and Engineering Sciences 465 (2111) (2009) 3517–3530. arXiv:http://rspa.royalsocietypublishing.org/content/465/2111/3517.full.pdf, doi:10.1098/rspa.2009.0307.
URL http://rspa.royalsocietypublishing.org/content/465/2111/3517

[32] D. J. Rayneau-Kirkhope, M. A. Dias, Recipes for selecting failure modes in 2-d lattices, Extreme Mechanics Letters 9 (2016) 11 – 20. doi:https://doi.org/10.1016/j.eml.2016.04.004.
URL http://www.sciencedirect.com/science/article/pii/S235243161630044X

[33] C. Borcea, I. Streinu, Geometric auxetics, Proceedings of the Royal Society of London A: Mathematical, Physical and Engineering Sciences 471 (2184). arXiv:http://rspa.royalsocietypublishing.org/content/471/2184/20150033.full.pdf, doi:10.1098/rspa.2015.0033.
URL http://rspa.royalsocietypublishing.org/content/471/2184/20150033

[34] D. Rayneau-Kirkhope, C. Zhang, L. Theran, M. A. Dias, Analytic analysis of auxetic metamaterials through analogy with rigid link systems, Proceedings of the Royal Society of London A: Mathematical, Physical and Engineering Sciences 474 (2210). arXiv:http://rspa.royalsocietypublishing.org/content/474/2210/20170753.full.pdf, doi:10.1098/rspa.2017.0753.
URL http://rspa.royalsocietypublishing.org/content/474/2210/20170753

[35] D. Jacobs, M. Thorpe, Generic rigidity percolation in two dimensions, Physical review. E, Statistical physics, plasmas, fluids, and related interdisciplinary topics 53 (1996) 3682–3693. doi:10.1103/PhysRevE.53.3682.

[36] A. Sartbaeva, S. A. Wells, M. M. J. Treacy, M. F. Thorpe, The flexibility window in zeolites., Nature materials 5 12 (2006) 962–5.

[37] Y.-H. Lee, K.-J. kang, A wire-woven cellular metal: Part-i, optimal design for applications as sandwich core, Materials & Design 30 (10) (2009) 4434 – 4443.

[38] S. Hyun, J.-E. Choi, K.-J. Kang, Effects of imperfections on the mechanical behavior of a wire-woven bulk Kagome cellular metal under compression, Computational Materials Science 46 (1) (2009) 73 – 82, https://note.org/10.1016/j.commatsci.2009.02.007.

[39] L. Feng, P. Alliez, L. Busé, H. Delingette, M. Desbrun, Curved optimal delaunay triangulation, ACM Trans. Graph 37 (4) (2018) 61:1–61:16.

[40] H. Si, Tetgen, a delaunay-based quality tetrahedral mesh generator, ACM Trans. Math. Softw. 41 (2) (2015) 11:1–11:36, 10.1145/2629697.
URL http://note.acm.org/10.1145/2629697

[41] G. Farin, Curves and Surfaces for Computer Aided Geometric Design: A Practical Guide, Academic Press, 1988.

[42] C. de Boor, B-form basics, in: G. Farin (Ed.), Geometric Modeling: Algorithms and New Trends, SIAM, 1987, pp. 131–148.

[43] T. W. Sederberg, S. R. Parry, Free-form deformation of solid geometric models, SIGGRAPH Comput. Graph. 20 (4) (1986) 151–160, 10.1145/15886.15903.
URL http://note.acm.org/10.1145/15886.15903

[44] M. Sitharam, M. Wang, How the beast really moves: Cayley analysis of mechanism realization spaces using caymos, Computer-Aided Design 46 (0) (2014) 205 – 210, 2013 SIAM Conference on Geometric and Physical Modeling.

[45] M. Wang, M. Sitharam, Algorithm 951: Cayley analysis of mechanism configuration spaces using caymos: Software functionalities and architecture, ACM Trans. Math. Softw. 41 (4) (2015) 27:1–27:8, 10.1145/2699462.

[46] M. Sitharam, H. Gao, Characterizing graphs with convex and connected configuration spaces, Discrete & Computational Geometry 43 (3) (2010) 594–625, 10.1007/s00454-009-9160-8.

[47] T. Baker, M. Sitharam, M. Wang, J. Willoughby, Optimal decomposition and recombination of isostatic geometric constraint systems for designing layered materials, Computer Aided Geometric Design 40 (2015) 1 – 25, https://note.org/10.1016/j.cagd.2015.07.001.

[48] C. M. Hoffman, A. Lomonosov, M. Sitharam, Decomposition plans for geometric constraint systems, part i: Performance measures for

cad, Journal of Symbolic Computation 31 (4) (2001) 367 – 408, https://note.org/10.1006/jsco.2000.0402.
[49] C. M. Hoffman, A. Lomonosov, M. Sitharam, Decomposition plans for geometric constraint problems, part ii: New algorithms, Journal of Symbolic Computation 31 (4) (2001) 409 – 427, https://note.org/10.1006/jsco.2000.0403.
[50] C. de Boor, K. Höllig, S. Riemenschneider, Box Splines, Springer-Verlag New York, Inc., New York, NY, USA, 1993.
[51] C. Loop, Smooth subdivision surfaces based on triangles, Ph.D. thesis, M.S. Mathematics thesis, University of Utah (1987).
[52] M. Kim, J. Peters, Symmetric box-splines on root lattices, J. Computational Applied Mathematics 235 (14) (2011) 3972–3989.
[53] Wikipedia contributors, Fáry's theorem— Wikipedia, the free encyclopedia, [Online; accessed 6-February-2019] (2018).
URL https://en.wikipedia.org/wiki/Fry%27s_theorem
[54] Wikipedia contributors, Tutte embedding— Wikipedia, the free encyclopedia, [Online; accessed 6-February-2019] (2019).
URL https://en.wikipedia.org/wiki/Tutte_embedding
[55] S. Gortler, Discrete one-forms on meshes and applications to 3d mesh parameterization, Computer Aided Geometric Design 23 (2006) 83–112, https://note.org/10.1016/j.cagd.2005.05.002.
[56] K. Wagner, Bemerkungen zum vierfarbenproblem, J. der Deutschen Mathematik 46 (1) (1963) 26–32.
[57] A. K. Dewdney, Wagner's theorem for torus graphs, Discrete Mathematics 4 (2) (1973) 139–149.
[58] S. Negami, A. Nakamoto, Diagonal transformations of graphs on closed surfaces, Sci Rep Yokohama Nat Univ Sect I Math Phys Chem 40.
[59] E. Osherovich, A. M. Bruckstein, All triangulations are reachable via sequences of edge-flips: an elementary proof, Computer Aided Geometric Design 25 (2008) 157–161.
[60] L. Asimow, B. Roth, The rigidity of graphs, Transactions of the American Mathematical Society 245 (1978) 279–289, http://dx.note.org/10.1090/S0002-9947-1978-0511410-9.
[61] J. C. Owen, Algebraic solution for geometry from dimensional constraints, in: Proceedings of the First ACM Symposium on Solid Modeling Foundations and CAD/CAM Applications, SMA '91, ACM, New York, NY, USA, 1991, pp. 397–407, 10.1145/112515.112573.
[62] B. Jackson, T. Jordán, Pin-collinear body-and-pin frameworks and the-molecular conjecture, Discrete & Computational Geometry 40 (2) (2008) 258–278, 10.1007/s00454-008-9100-z.
[63] R. Haas, D. Orden, G. Rote, F. Santos, B. Servatius, H. Servatius, D. Souvaine, I. Streinu, W. Whiteley, Planar minimally rigid graphs and pseudo-triangulations, Computational Geometry 31 (1) (2005) 31 – 61, special Issue on the 19th Annual Symposium on Computational Geometry - SoCG 2003.
URL http://www.sciencedirect.com/science/article/pii/S0925772104001063
[64] H. Pollaczek-Geiringer, Uber die Gliederung ebener Fachwerke, ZAMM - Journal of Applied Mathematics and Mechanics / Zeitschrift für Angewandte Mathematik und Mechanik 7 (1) (1927) 58–72, 10.1002/zamm.19270070107.
URL http://dx.note.org/10.1002/zamm.19270070107
[65] G. Laman, On graphs and rigidity of plane skeletal structures, Journal of Engineering Mathematics 4 (1970) 331–340, 10.1007/BF01534980.
[66] T.-S. Tay, W. Whiteley, Recent advances in the generic rigidity of structures, Structural Topology 9 (1984) 31–38, dual French-English text.
[67] W. Whiteley, A matroid on hypergraphs, with applications in scene analysis and geometry, Discrete & Computational Geometry 4, https://note.org/10.1007/BF02187716.
[68] W. Whiteley, Some matroids from discrete applied geometry, Matroid Theory 197.
[69] L. Theran, A. Nixon, E. Ross, M. Sadjadi, B. Servatius, M. F. Thorpe, Anchored boundary conditions for locally isostatic networks, Phys. Rev. E 92 (2015) 053306, 10.1103/PhysRevE.92.053306.
[70] A. Lee, I. Streinu, L. Theran, Graded sparse graphs and matroids., J. UCS 13 (11) (2007) 1671–1679.
[71] D. J. Jacobs, B. Hendrickson, An algorithm for two-dimensional rigidity percolation: The pebble game, Journal of Computational Physics 137 (2) (1997) 346 – 365.
[72] H.-S. Ahn, A physical interpretation of the rigidity matrix, 2017 IFAC WC Workshop Rigidity Theory for Multi-agent Systems Meets Parallel Robots Towards the Discovery of Common Models and Methods (2017).
URL https://parrigidwrkshp.sciencesconf.org/data/pages/IFAC2017_parrigid_02_Ahn.pdf
[73] R. Connelly, A. Back, Mathematics and tensegrity, American Scientist 86 (1998) 142.
[74] X. Ni, A. Al, A. Khanikaev, Topological edge states of distorted photonic Kagome lattices, in: Active Photonic Platforms IX, 2017, p. 56, 10.1117/12.2273938.
[75] X. Ni, M. A. Gorlach, A. Alu, A. B. Khanikaev, Topological edge states in acoustic Kagome lattices, New Journal of Physics 19 (5) (2017) 055002.
[76] M. Sitharam, J. Youngquist, M. Nolan, J. Peters, Slicing cost microstructure, uRL: https://www.youtube.com/watch?v=pjOmRuwIzWs. Last visited 2019-04-25 (2019).
[77] M. Ostoja-Starzewski, Material spatial randomness: from statistical to representative volume element, Probab. Eng. Mech. 21 (2) (2006) 112–132.